ISSN 2635-1676, Nanobiotechnology Reports, 2023, Vol. 18, Suppl. 1, pp. S101–S109. © Pleiades Publishing, Ltd., 2023.

NANOMATERIALS FOR FUNCTIONAL AND STRUCTURAL PURPOSES

Synthesis, Structure, and Thermoelectric Properties of Holmium-Doped Nanomaterials Based on Bismuth Telluride

M. N. Yapryntsev[a],* and O. N. Ivanov[a]

[a] *Federal State Autonomous Educational Institution of Higher Education "Belgorod National Research University," Belgorod, 308015 Russia*

**e-mail: yaprintsev@bsu.edu.ru*

Received April 24, 2023; revised May 15, 2023; accepted May 15, 2023

Abstract—Powdered thermoelectric materials $Bi_{2-x}Ho_xTe_{2.7}Se_{0.3}$ (x = 0, 0.001, 0.0025, 0.005, 0.01, and 0.02) are obtained by the method of solvothermal synthesis. The possibility of obtaining nanomaterials based on holmium-doped bismuth telluride is shown. The influence of the concentration of holmium on the parameters of the crystal lattice, morphology and average size of the synthesized particles are studied. Bulk materials $Bi_{2-x}Ho_xTe_{2.7}Se_{0.3}$ are obtained by spark plasma sintering. All obtained samples are textured, the crystallographic axis of the texture (0 0 *l*) is directed parallel to the direction of the application of pressure during compaction. Development of the texture is confirmed by scanning electron microscopy and X-ray diffraction (XRD) analysis. The grains in the textured samples form an ordered lamellar structure, and the lamellar sheets lie in the plane perpendicular to the direction of pressing. An increase in the concentration of holmium leads to an increase in the degree of texturing. The thermoelectric properties of the bulk materials $Bi_{2-x}Ho_xTe_{2.7}Se_{0.3}$ are also obtained

DOI: 10.1134/S2635167623600980

INTRODUCTION

The main microstructural and nanostructural features of polycrystalline materials are determined by the shape, size, and dimension of crystallites (grains) and the ordering of grains (presence and degree of texturing) [1–3]. Intergrain boundaries in polycrystalline materials are scattering centers for both electrons, which affects the electrical resistance, and phonons, which affects the thermal conductivity [4–7]. These transport properties are one of the main thermoelectric properties of materials that determine their thermoelectric figure of merit. The formation of a grain structure in a thermoelectric material with necessary microstructural or nanostructural characteristics provides an additional opportunity for optimizing the transport properties and increasing the thermoelectric figure of merit. As the grain size decreases, the efficiency of the grain boundaries as scattering centers for electrons and phonons increases, which leads to the appearance of size effects in the electrical resistance and thermal conductivity, usually observed when the grain size decreases from the microrange to nanorange (~100 nm) [8, 9]. An effective method for producing materials with a controlled grain structure and the required grain size is based on synthesis of the initial powder and its subsequent high-temperature sintering into a bulk and mechanically strong material. Obviously, to obtain a bulk material with a nanograin structure, the initial powder must also be nanoscale, i.e., consist of particles smaller than ~100 nm. The problem is that high-temperature grain growth during the sintering of a polycrystalline material from an initial nanoscale powder, as a rule, does not allow a nanograin structure to be obtained. To prevent grain growth beyond the nanoscale determined by the particle size in the initial powder, various techniques are used that are based on the introduction of special additives into the sintered initial powder that prevent grain growth (growth inhibitors) and optimization of the sintering process by reducing the temperature and the sintering time when using such methods such as spark plasma sintering (SPS), reactive SPS, etc. [10–13].

The purpose of this work is to demonstrate and analyze the effect of a decrease in grain size from the microscale to nanoscale and the concomitant effect of an increase in the degree of grain ordering upon sequential doping of $Bi_2Te_{2.7}Se_{0.3}$ compound samples with holmium obtained using SPS of the corresponding initial powders. Currently, the compound $Bi_2Te_{2.7}Se_{0.3}$ is widely used for the manufacture of electronic-conductivity legs in low-temperature thermoelectric devices [14].

EXPERIMENTAL

To obtain samples of the $Bi_{2-x}Ho_xTe_{2.7}Se_{0.3}$ compound with different dopant contents (x = 0, 0.001, 0.0025, 0.005, 0.01, and 0.02), methods of solvothermal synthesis (to obtain the initial powders) and SPS (to obtain the bulk materials) were used. To synthesize the initial powders, we used the analytically pure chemical substances ($Bi(NO_3)_3{\cdot}5H_2O$, TeO_2, SeO_2, $Ho(NO_3)_3{\cdot}6H_2O$, NaOH, and ethane-1,2-diol. At the first stage of synthesis ($Bi(NO_3)_3{\cdot}5H_2O$, TeO_2, SeO_2, and $Ho(NO_3)_3{\cdot}6H_2O$, taken per 30 g of the product in a stoichiometric ratio corresponding to the required x value, were dissolved in a mixture of 1000 cm^3 of ethane-1,2-diol and 20 g of NaOH with vigorous stirring using a magnetic stirrer. After complete dissolution, the volume of the reaction medium was brought to 1500 cm^3 with ethane-1,2-diol, then heated to boiling point. Upon intensive boiling, the system was kept open for 15 min to remove water, then the system was equipped with a reflux condenser and a water seal to prevent contact with atmospheric oxygen. Isothermal exposure was carried out at a temperature of 185°C for 6 h, then the system was naturally cooled to room temperature. After the end of the reaction, the dark-gray precipitate was separated by centrifugation, washed several times with isopropyl alcohol, and then dried at 80°C for 8 h in air.

To obtain bulk materials, the SPS of the synthesized initial powders was carried out using a SPS installation, model 10-3. The powders were poured into a graphite mold with an internal diameter of 20 mm, sintering was carried out in a vacuum chamber with a residual pressure of 1.5 Pa, at a pressing pressure of 40 MPa, and temperature of 680 K for 2 min.

The density of the bulk samples was determined using the Archimedes method. To determine the crystal structure and phase composition of the initial powders and bulk materials, X-ray phase analysis (XPA, SmartLab 9kW X-ray diffractometer with CuK_α radiation) was performed. Scanning electron microscopy (SEM, Nova NanoSEM 450 microscope) was employed to study the morphology and estimate the particle size of the initial powders and study the characteristics of the grain structure of the bulk materials. An ICPE-9000 inductively coupled plasma optical emission spectrometer was used to determine the exact elemental composition of the samples with different Ho content. The ZEM-3 system was used to measure the electrical resistivity using the four-probe method, and the TC-1200Rh system was used to measure the total thermal conductivity using the laser flash method. Next, using the Wiedemann–Franz law and using electrical-resistivity values, the phonon contribution to the total thermal conductivity was determined. The measurement errors were ~1% when measuring the electrical resistivity and ~5% when measuring the total thermal conductivity.

RESULTS AND DISCUSSION

It follows from the XPA results that all initial powders of the $Bi_{2-x}Ho_xTe_{2.7}Se_{0.3}$ compound with different Ho content are single phase and correspond to the $Bi_2Te_{2.7}Se_{0.3}$ compound (PDF card no. 01-089-2009). A typical diffraction pattern of the initial powder with the composition of $Bi_{1.995}Ho_{0.005}Te_{2.7}Se_{0.3}$ is shown in Fig. 1a. All diffraction peaks were accurately indexed according to the $R\bar{3}m$ space group. For initial powders with different x, the unit-cell parameters c (curve *1* in Fig. 2) and $a = b$ (curve *2*) were determined using the internal standard method. It can be seen that with increasing Ho concentration, a gradual decrease in the crystal-lattice parameters is observed, which may be due to the difference in the atomic radii of bismuth ($R(Bi^{3+}) = 0.102$ nm) as an atom of the main substance and holmium ($R(Ho^{3+}) = 0.093$ nm) as an impurity atom that replaces bismuth during doping [15]. According to optical-emission-spectrometry data, the real elemental composition of the initial powders of the $Bi_{2-x}Ho_xTe_{2.7}Se_{0.3}$ compound with different x corresponded to the nominal composition.

All the initial powders consisted of particles in the shape of thin hexagonal plates. A SEM image of particles of the initial powder with the composition $Bi_{1.995}Ho_{0.005}Te_{2.7}Se_{0.3}$ is shown in Fig. 3. The formation of hexagonal plates is associated with the features of the crystal structure and chemical bonds characteristic of compounds based on Bi_2Te_3 [16, 17]. The crystallographic plane a–b coincides with the plane of the plates, and the crystallographic axis c is directed perpendicular to this plane. To estimate the average particle size using SEM images obtained for each composition, histograms of the particle size distribution were constructed. Histograms were analyzed within the framework of the unimodal lognormal distribution [18]. The obtained dependences of d and h on the Ho content are shown in Fig. 4. It can be seen that the transverse particle size gradually decreases with increasing x, while the particle thickness varies very slightly and nonmonotonically depending on the Ho content. It is important to note that the dimensions d correspond to the microrange, and h, to the nanorange. Thus, all initial powders of the $Bi_{2-x}Ho_xTe_{2.7}Se_{0.3}$ compound with different Ho contents are nanoscale. The change in dimensions d and h caused by Ho doping leads to a gradual change in the particle shape, which can be quantitatively characterized by the particle shape factor, defined as the ratio d/h. The larger this ratio, the higher the anisotropy of the particle shape. The dependence of d/h on the Ho content is shown in the inset to Fig. 4. For all compositions, $d \gg h$, i.e., the particles in the initial powders are highly anisotropic in shape. However, the particle shape factor gradually

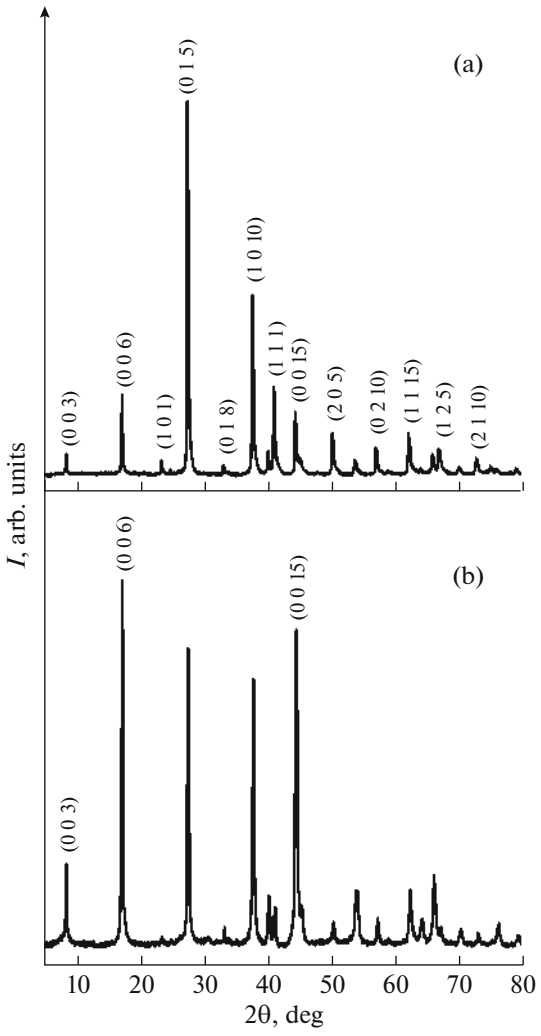

Fig. 1. X-ray diffraction pattern of the initial powder (a) and bulk material (b) of the composition $Bi_{1.995}Ho_{0.005}Te_{2.7}Se_{0.3}$.

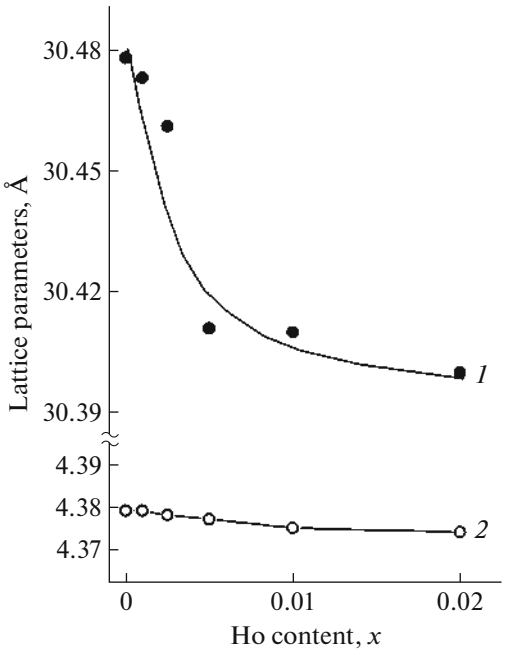

Fig. 2. Effect of holmium doping on the crystal-lattice parameters c (*1*) and $a = b$ (*2*) of the $Bi_{2-x}Ho_xTe_{2.7}Se_{0.3}$ compound.

decreases from the maximum value of ~7.4 for $x = 0.0$ to ~4.9 for $x = 0.02$. This decrease in the particle shape anisotropy with a gradual increase in the doping level is only due to the *d(x)* dependence, since the particle thickness is practically independent of x. A decrease in the transverse particle size in the initial powders synthesized by the solvothermal method as a result of doping with rare-earth Sm was previously discovered for the compound $Bi_{2-x}Sm_xTe_{2.7}Se_{0.3}$ [19]. This effect of doping on the particle size was explained as a consequence of a change in the degree of polarity of the covalent-polar bond (or the degree of ionicity of the *IF* bond) upon the partial replacement of bismuth atoms with samarium atoms. A similar mechanism for changing the degree of ionicity of a bond can be used to explain the decreasing $d(x)$ dependence for the $Bi_{2-x}Ho_xTe_{2.7}Se_{0.3}$ compound. It must be taken into account that the synthesis of the initial powders of this compound with different Ho contents was carried out in ethane-1,2-diol, which is a polar solvent. In addition, compounds based on Bi_2Te_3 have a layered structure, and the interaction between Bi and Te atoms within the layers occurs through a covalently polar chemical bond, i.e., these compounds have the properties of ionic crystals, depending on the degree of ionicity of the covalently polar bonds. In the general case, the formation of particles during synthesis of the initial powders in polar solvents is determined by the kinetics of two simultaneously operating processes: the process of the deposition of ions of the growing substance on the nuclei of forming particles, which leads to an increase in the particle size, and the process of the dissolution of particles, which leads to a decrease in their size [20–22]. That is, the average particle size is determined as a result of the dynamic equilibrium of two simultaneously, but oppositely acting processes. Shifting this balance in any direction will lead to the establishment of a new equilibrium, which will be characterized by a different average particle size. The decrease in the transverse size d observed with increasing Ho concentration in the $Bi_{2-x}Ho_xTe_{2.7}Se_{0.3}$ compound may be a consequence of a change in the degree of ionicity of the covalently polar $Bi_{2-x}(Ho_x)$–Te bond (when calculating its degree of ionicity, it is also necessary to take into account the partial replacement of Te by Se in this bond). The change in the degree of ionicity of the *IF* bond upon doping with Ho may be associated with a difference in the electronegativities of Bi and Ho atoms ($X_{Ho} = 1.23$ and $X_{Bi} = 2.02$ [23]). The change in

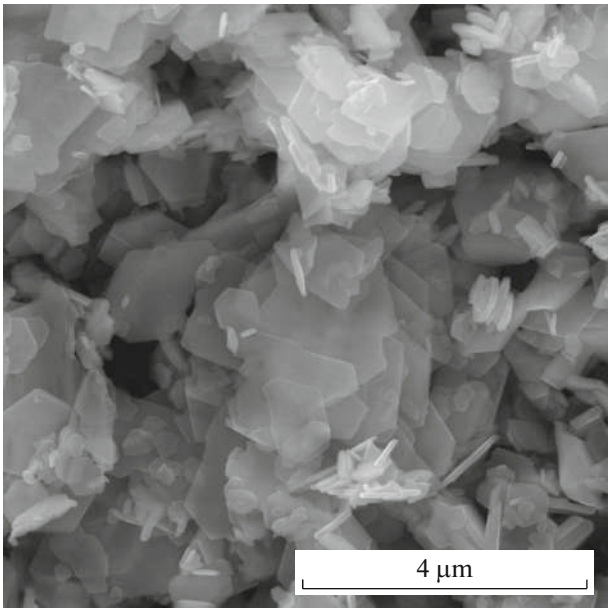

Fig. 3. SEM image of particles of the initial powder of the composition $Bi_{1.995}Ho_{0.005}Te_{2.7}Se_{0.3}$.

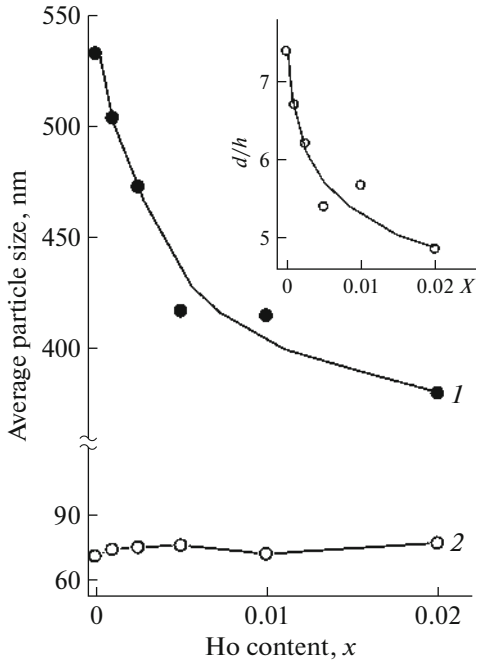

Fig. 4. Effect of holmium doping on the average values of the transverse size d (*1*) and thickness h (*2*) of particles in the initial powders of the $Bi_{2-x}Ho_xTe_{2.7}Se_{0.3}$ compound. The inset shows the dependence of the particle shape factor d/h on the doping level.

the degree of ionicity of a bond can be assessed using Pauling's equation [24]:

$$IF = 1 - \left[\exp\left\{-\frac{(\Delta X)^2}{4}\right\}\right] \times 100\ \%, \qquad (1)$$

where X_A and X_B are the electronegativity of atoms (ions) interacting through a covalently polar bond, $\Delta X = X_A - X_B$.

To take into account the effect of Ho doping on a change in the degree of ionicity of the $Bi_{2-x}(Ho_x)$–Te bond, the value of its relative change (relative to the value for the undoped sample) was used, introduced as follows: $IFR(x) = IF(x)/IF(x = 0)$. The $IFR(x)$ dependence is shown in Fig. 5. As x increases, the degree of ionicity of the $Bi_{2-x}(Ho_x)$–Te bond increases linearly. It is known that with an increase in the degree of ionicity of chemical bonds, the solubility of substances with this type of bond in polar solvents increases [20–22]. An increase in *IFR* shown in Fig. 5 as a result of doping makes the process of the dissolution of particles of the $Bi_{2-x}Ho_xTe_{2.7}Se_{0.3}$ compound formed during solvothermal synthesis more efficient, which leads to a corresponding decrease in the average particle size in the synthesized initial powders (inset in Fig. 5). We note that the $Bi_{2-x}(Ho_x)$–Te bonds act precisely in the plane of growing hexagonal particles, which leads to the effect of doping only on the transverse particle size. In the perpendicular direction, the weak van der Waals interaction, which is not sensitive to doping, is responsible for the interaction of atoms, so the thickness of the particles barely changes with increasing x.

The features of the morphology of particles of the initial powders of the $Bi_{2-x}Ho_xTe_{2.7}Se_{0.3}$ compound (thin plates with a large value of the particle shape factor, the value of which depends on the doping level) have a significant impact on the features of the morphology of the grain structure of bulk samples obtained from the corresponding initial powders. The density of the bulk samples did not depend on the Ho content and was equal to ~7.5 g/cm^3, which is ~96% of the theoretical density (7.78 g/cm^3).

It was found that all bulk samples are textured during the SPS process. The ordering of grains during texturing is determined both by the shape of the particles in the initial powders and by the action of uniaxial pressure on these particles during the SPS process [25]. The grains in the bulk samples have the shape of plates, the transverse size of which significantly exceeds their thickness. The crystallographic plane a–b coincides with the basal surface of the lamellar grains, and the crystallographic axis c is perpendicular to this surface. During texturing, grains are arranged into lamella layers oriented perpendicular to the direction of the application of pressure during the SPS process. This direction is the texture axis. The listed features of the grain structure, caused by texturing, are observed in the SEM images obtained from the planes oriented perpendicularly ("perpendicular" plane) or parallel ("parallel" plane) to the texture axis. As an

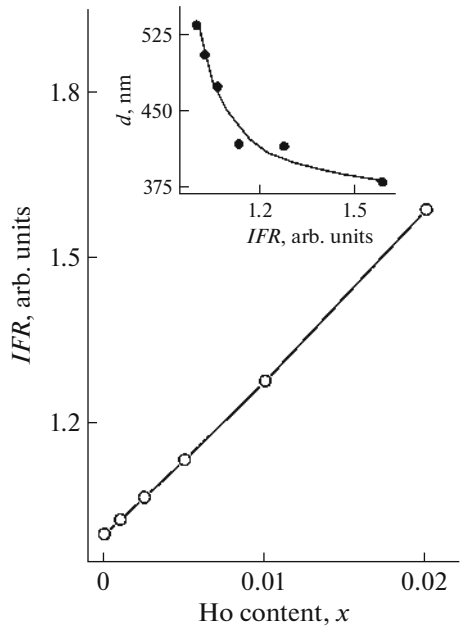

Fig. 5. Effect of holmium doping on the degree of ionicity of the covalently polar $Bi_{2-x}(Ho_x)$–Te *IFR* bond in the $Bi_{2-x}Ho_xTe_{2.7}Se_{0.3}$ compound. The inset shows the dependence of the average transverse particle size *d* on the degree of bond ionicity.

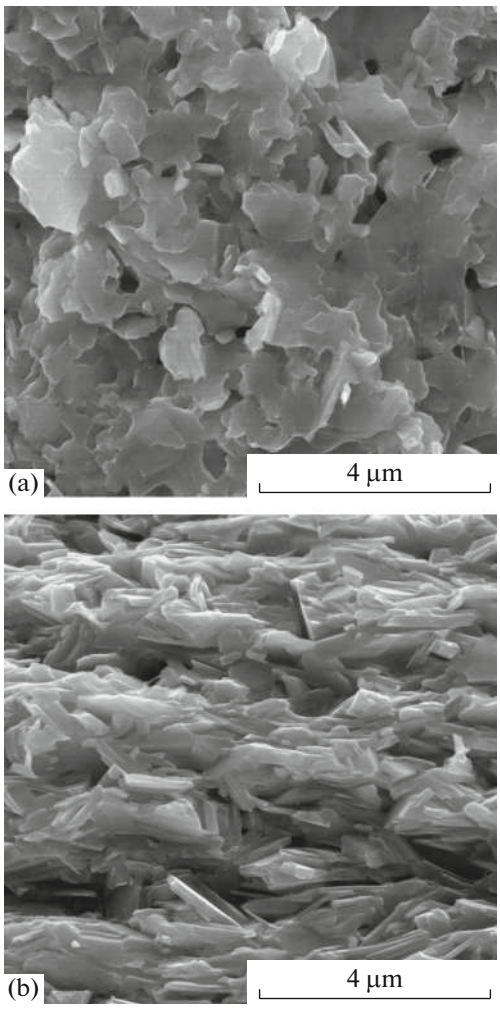

Fig. 6. SEM images of the surfaces of a sample of the composition $Bi_{1.995}Ho_{0.005}Te_{2.7}Se_{0.3}$ oriented perpendicular (a) and parallel (b) to the direction of pressing during the SPS process.

example, such images for the composition $Bi_{1.995}Ho_{0.005}Te_{2.7}Se_{0.3}$ are shown in Fig. 6. On the perpendicular surface, the grain structure is represented by chaotically oriented grains of irregular shape (view of the lamellar grains of the lamellar layers from top). The parallel surface shows grains arranged in lamellar layers (side view of lamellar grains).

In addition, texturing in the samples of the $Bi_{2-x}Ho_xTe_{2.7}Se_{0.3}$ compound is observed in X-ray diffraction patterns obtained from the perpendicular and parallel planes. The diffraction pattern of the perpendicular surface of the sample with the composition $Bi_{1.995}Ho_{0.005}Te_{2.7}Se_{0.3}$ is shown in Fig. 1b. Although all the peaks in the diffraction pattern can be attributed to the rhombohedral structure $R\bar{3}m$, the intensities of the (00*l*) peaks increase markedly relative to the intensities of the same peaks in the diffraction pattern of the corresponding initial powder. This redistribution of peak intensities is consistent with the formation of a texture with the predominant ordering of grains in the plane perpendicular to the pressing direction. The degree of preferred grain orientation was assessed using the Lotgering *LF* method [26]. The *LF*(*x*) dependence, showing an increase in the degree of texturing with increasing Ho concentration, is shown in Fig. 7.

As for the particles of the initial powders, SEM images of perpendicular and parallel surfaces were used to construct histograms of the grain-size distribution (obviously, in the case of a perpendicular surface this size corresponds to the transverse grain size, and in the case of a parallel surface, to the grain thickness), and for subsequent determination of the average values of the transverse size *D* and thickness *H*, and the grain-shape factor *D*/*H*. The dependences *D*(*x*) and *H*(*x*) are presented in Fig. 8 by curves *1* and *2*, respectively, the inset to this figure shows the dependence $D/H = f(x)$. It can be seen that, firstly, the transverse size and thickness of grains in the bulk samples are much larger than the transverse size and thickness of particles in the corresponding initial powders and, secondly, *D* and *H* decrease significantly with increasing Ho content (i.e., qualitatively, the dependence of *D*(*x*) is consistent with the dependence *d*(*x*), but in contrast to the very weak dependence *h*(*x*), the dependence *H*(*x*) is clearly expressed). We note that the grain-shape factor increases with *x*. This dependence

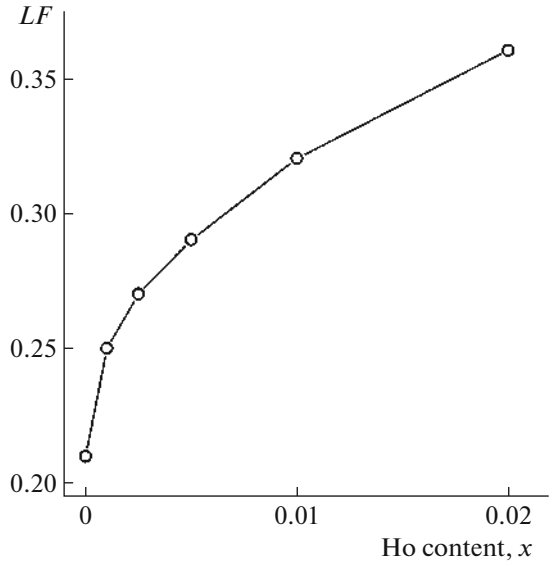

Fig. 7. Effect of holmium doping on the Lotgering factor *LF* of the samples of the $Bi_{2-x}Ho_xTe_{2.7}Se_{0.3}$ compound.

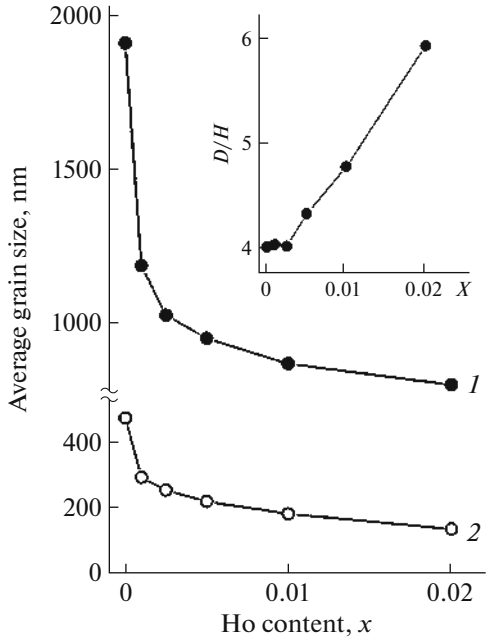

Fig. 8. Effect of holmium doping on the average values of the transverse size *D* (*1*) and thickness *H* (*2*) of grains in bulk samples of the $Bi_{2-x}Ho_xTe_{2.7}Se_{0.3}$ compound. The inset shows the dependence of the grain shape factor *D*/*H* on the doping level.

is associated with the kinetic features of the grain-growth process during sintering.

An increase in the grain size in bulk materials during sintering of the corresponding initial powders is a well-known phenomenon caused by a decrease in the energy of the system (sintered material) having numerous interfaces (grain boundaries). The energy of interfaces can be expressed as γA, where γ is the specific surface energy and A is the surface area. During the sintering process, the initial powder particles may retain their shape, but due to particle coalescence, their size will increase to reduce the surface area of the sintered particles. The increase in particle size depending on the sintering time at constant temperature can be expressed using [27]:

$$\bar{D}_t^n - \bar{D}_0^n = Ct\exp\left(-\frac{E_a}{RT}\right), \qquad (2)$$

where $\bar{D}_t$ and $\bar{D}_0$ are the average grain size at the time t and the initial grain size, respectively, E_a is the activation energy for grain growth, R is the universal gas constant, and n and C are constants.

If we assume that $\bar{D}_t = D$ (or H) and $\bar{D}_0 = d$ (or h), then we can introduce the average grain growth rates as follows: the average rate of increase in the transverse size of the grains is the transverse speed $(D-d)/\Delta t$ and the rate of increase in the grain thickness is the longitudinal speed $(H-h)/\Delta t$ ($\Delta t = 2$ min is the SPS duration). The effect of the doping level on these rates is shown in Fig. 9. As x increases, the transverse velocity constantly decreases, while the longitudinal velocity initially decreases sharply for $x = 0.001$, and with a further increase in x depends very little on the doping level. A decrease in the grain growth rates with increasing doping level in the $Bi_{2-x}Ho_xTe_{2.7}Se_{0.3}$ compound indicates an increase in the activation energy of grain growth. This effect of doping on grain growth can be explained if we assume that the segregation of Ho atoms occurs on the surfaces of particles of the initial powders, leading to the formation of holmium nanoinclusions. During the SPS process, these nanoinclusions can act as grain growth inhibitors. As the Ho content increases, the amount of such inhibitors will increase, which will lead to a slowdown in the grain growth rate and, consequently, to a decrease in the average grain size with increasing x.

The assumption of the formation of Ho nanoinclusions on the surface of particles of initial powders of the $Bi_{2-x}Ho_xTe_{2.7}Se_{0.3}$ compound can also be used to explain the increase in the Lotgering factor, which characterizes the degree of grain ordering with increasing doping level (Fig. 7). Such nanoinclusions can act as a "lubricant" during the packing of particles under the influence of uniaxial pressure during the SPS process of the original powders. The lubrication effect was indeed found for some systems (the effect of Ce nanoinclusions as a lubricant for Al_2O_3 [28] and the effect of Te nanoinclusions as a lubricant for Bi_2Te_3 [29]). The presence of a lubricant makes the particle packing process more efficient, i.e., the degree of the ordered arrangement of lamellar particles in the plane perpendicular to the direction of the application of pressure increases, which will then lead to a corre-

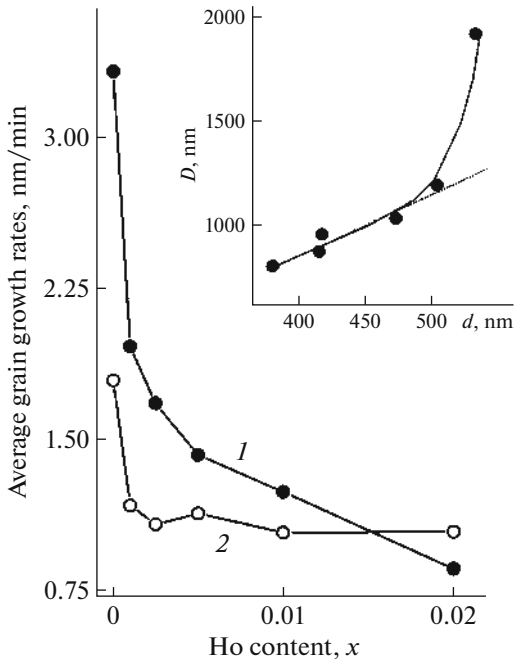

Fig. 9. Effect of holmium doping on the average values of the transverse (*1*) and longitudinal (*2*) grain growth rates in bulk samples of the $Bi_{2-x}Ho_xTe_{2.7}Se_{0.3}$ compound during the SPS process. The inset shows the relationship between the average transverse particle size d in the initial powders and the average transverse grain size D in the corresponding bulk materials.

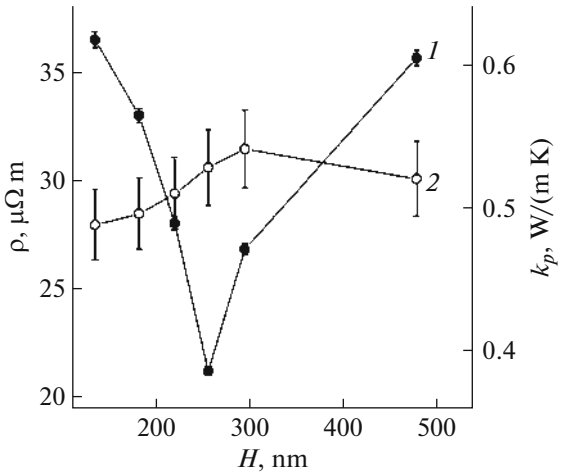

Fig. 10. Dependences of the electrical resistivity (*1*) and phonon contribution to the total thermal conductivity (*2*) for bulk samples of the $Bi_{2-x}Ho_xTe_{2.7}Se_{0.3}$ compound.

sponding increase in the degree of ordering of grains in bulk materials. Thus, an increase in lubrication centers on the surface of the particles of the initial powders should lead to an increase in the degree of packing of the particles and a subsequent increase in the degree of texturing of the polycrystalline material obtained from this initial powder. If we assume that the lubricating centers are holmium nanoinclusions in the $Bi_{2-x}Ho_xTe_{2.7}Se_{0.3}$ compound, then the number of such centers will increase with increasing doping level and, consequently, the degree of texturing of bulk samples will increase. This dependence was discovered experimentally (Fig. 7).

The inset in Fig. 9 shows the relationship between the average transverse particle size in the initial powders and the average transverse grain size in the corresponding bulk materials. It can be seen that, with the exception of the maximum values of these sizes, the presented dependence is linear, i.e., an increase in the particle size leads to a directly proportional increase in the grain size.

As follows from Fig. 8, as x increases, the average grain thickness in bulk samples of the $Bi_{2-x}Ho_xTe_{2.7}Se_{0.3}$ compound gradually decreases from ~480 nm for $x = 0$ to ~130 for $x = 0.2$, i.e., doping with holmium causes a gradual transition of the grain structure from the microrange to the nanorange. Since intergranular grains particles are scattering centers for electrons and phonons; such a transition can be accompanied by the appearance of size effects in the electrical resistivity ρ and the phonon contribution to the thermal conductivity k_p. The dependences of ρ and k_p on the average grain thickness, taken for the samples under study at room temperature, are shown in Fig. 10. These dependences are nonmonotonic, but the most important thing is that ρ increases and k_p decreases with a gradual decrease in H and transition to the nanorange. This behavior indicates the appearance of size effects in the transport properties of samples of the $Bi_{2-x}Ho_xTe_{2.7}Se_{0.3}$ compound with different grain thicknesses, which is determined by the doping level.

The observed size effects are caused by the additional scattering of electrons, leading to a decrease in their mobility, and phonons at grain boundaries. The dependence of the electron mobility on the average grain size $\bar{D}$ can be described by the expression [30]:

$$\mu_b = \frac{l_e/\bar{D}}{1 + l_e/\bar{D}}\mu_a, \quad (3)$$

where μ_a is the mobility of the bulk material (i.e., without taking into account the scattering of electrons at grain boundaries) when taking into account the scattering of electrons by acoustic phonons and l_e is the mean free path of the electron.

The dependence of the phonon contribution to the total thermal conductivity on the average grain size can be represented by the expression [30]:

$$k_p = k_s - \frac{2}{3}k_0\sqrt{\frac{l_0}{\bar{D}}}, \quad (4)$$

where k_s and k_0 are the lattice contributions to thermal conductivity for a heavily doped semiconductor and a pure crystal, l_0 is the mean free path of a phonon.

In heavily doped semiconductors, short-wavelength phonons are strongly scattered by point defects, so long-wavelength phonons make the largest contribution to the thermal conductivity. Therefore, in order for the effect of phonon scattering at grain boundaries on the phonon contribution to the total thermal conductivity to be noticeable at room temperature, it is necessary to use a heavily doped semiconductor.

In accordance with expressions (3) and (4), as the average grain size decreases, ρ should increase, and k_p should increase, which was observed in the experiment.

We note that the effect of doping on the transport properties of polycrystalline semiconductors can be associated not only with size effects, but also with a change in the degree of texturing, as well as with a change in the concentration of conduction electrons (it is known [31–35] that rare-earth elements are donor-type impurities in the compounds based on Bi_2Te_3). However, the degree of texturing of the $Bi_{2-x}Ho_xTe_{2.7}Se_{0.3}$-compound samples increases all the time with increasing doping level (Fig. 7), which does not agree with the data in Fig. 10. The concentration of conduction electrons should also increase with increasing x, which should lead to a consistent decrease in the electrical resistivity. Therefore, namely size effects were used to explain the characteristic features of the transport properties of samples of the $Bi_{2-x}Ho_xTe_{2.7}Se_{0.3}$ compound.

CONCLUSIONS

Doping of the compounds based on Bi_2Te_3 with rare-earth elements is usually used to improve the thermoelectric properties of compounds through traditional mechanisms of doping influence (main mechanisms: formation of point defects acting as scattering centers for electrons and phonons, formation of impurity resonant energy levels) [31–35]. It follows from the results of this work that doping with holmium allows one not only to influence the thermoelectric properties of the $Bi_2Te_{2.7}Se_{0.3}$ compound through traditional mechanisms, but also to simultaneously lead to a decrease in grain size and an increase in the degree of texturing of bulk samples of this compound, which can facilitate the implementation of additional size effects in transport thermoelectric properties.

FUNDING

The work was carried out with financial support of the Russian Science Foundation (grant no. 21-73-00199) using equipment of the Center for Collective Use of Scientific Equipment "Technologies and Materials" of the Federal State Autonomous Educational Institution of Higher Education "Belgorod National Research University."

CONFLICT OF INTEREST

The authors of this work declare that they have no conflicts of interest.

REFERENCES

1. D. Wolf, J. Lutsko, and M. Kluge, "Physical Properties of Grain-Boundary Materials: Comparison of EAM and Central-Force Potentials," in *Atomistic Simulation of Materials*, Ed. by V. Vitek and D. J. Srolovitz (Springer, Boston, 1989).
2. T. Watanabe, J. Mater. Sci. **46**, 4095 (2011). https://doi.org/10.1007/s10853-011-5393-z
3. I. P. Semenova, R. Z. Valiev, E. B. Yakushina, et al., J. Mater. Sci. **4**, 7354 (2008). DOI: 8-2984-4 https://doi.org/10.1007/s10853-00
4. A. J. Minnich, M. S. Dresselhaus, Z. F. Ren, et al., Energy Environ. Sci. **2**, 466 (2009). https://doi.org/10.1039/b822664b
5. M. G. Kanatzidis, Chem. Mater. **22**, 648 (2009). https://doi.org/10.1021/cm902195j
6. Z. G. Chen, G. Han, L. Yang, et al., Prog. Nat. Sci. Mater. Int. **22**, 535 (2012). https://doi.org/10.1016/j.pnsc.201P2.11.011
7. O. N. Ivanov, M. N. Yapryntsev, A. E. Vasil'ev, and N. I. Repnikov. Ross. Nanotekhnol. **16**, 348 (2021). https://doi.org/10.1134/S1992722321030079
8. O. Ivanov, O. Maradudina, and R. Lyubushkin, Mater. Charact. **99**, 175 (2015). https://doi.org/10.1016/j.matchar.2014.12.001
9. Y. Xia, J. Park, F. Zhou, et al., Phys. Rev. Appl. **11**, 024017 (2019). https://doi.org/10.1103/PhysRevApplied.11.024017
10. M. Yaprintsev, A. Vasil'ev, and O. Ivanov, J. Eur. Ceram. Soc. **40**, 742 (2020). https://doi.org/10.1016/j.jeurceramsoc.2018.12.041
11. X. F. Wei, et al., J. Eur. Ceram. Soc. **40**, 935 (2020). https://doi.org/10.1016/j.jeurceramsoc.2019.12.034
12. J. H. Lee, I. H. Oh, and H. K. Park, Arch. Metall. Mater. **66**, 1029 (2021). https://doi.org/10.24425/amm.2021.136419
13. S. G. Huang, et al., Int. J. Refract. Hard Met. **26**, 389 (2008). https://doi.org/10.1016/j.ijrmhm.2007.09.003
14. H. J. Goldsmid, Materials **7**, 2577 (2014). https://doi.org/10.3390/ma7042577
15. Y. Q. Jia, Solid State Chem. **95**, 184 (1991). https://doi.org/10.1016/0022-4596(91)90388-X
16. J. R. Drabble and C. H. L. Goodman, J. Phys. Chem. Solids **5**, 142 (1958). https://doi.org/10.1016/0022-3697(58)90139-2
17. S. Nakajima, J. Phys. Chem. Solids **24**, 479 (1963). https://doi.org/10.1016/0022-3697(63)90207-5
18. F. J. Humphreys and M. Hatherly, *Recrystallization and Related Annealing Phenomena* (Elsevier, Oxford, 2004). https://doi.org/10.1016/C2009-0-07986-0

19. M. Yaprintsev, A. Vasil'ev, O. Ivanov, and D. Popkov, J. Solid State Chem. **312**, 123176 (2022). https://doi.org/10.1016/j.jssc.2022.123176
20. M. N. Joswiak, M. F. Doherty, and B. Peters, Proc. Natl. Acad. Sci. **115**, 656 (2018). https://doi.org/10.1073/pnas.1713452115
21. L. J. Wang, J. W. Lu, F. S. Xu, and F. S. Zhang, Chin. Sci. Bull. **56**, 713 (2011). https://doi.org/10.1007/s11434-010-4184-2
22. M. Kowacz, M. Prieto, and A. Putnis, Geochim. Cosmochim. Acta **74**, 469 (2010). https://doi.org/10.1016/j.gca.2009.10.028
23. G. D. Sproul, ACS Omega **5**, 11585 (2020). https://doi.org/10.1021/acsomega.0c00831
24. R. T. Sanderson, J. Am. Chem. Soc. **105**, 2259 (1983). https://doi.org/10.1021/ja00346a026
25. O. Ivanov, M. Yaprintsev, and A. Vasil'ev, J. Solid State Chem. **290**, 121559 (2020). https://doi.org/10.1016/j.jssc.2020.121559
26. F. K. Lotgering, J. Inorg. Nucl. Chem. **9**, 113 (1959). https://doi.org/10.1016/0022-1902(59)80070-1
27. J. Burke and D. Turnbull, Prog. Metal. Phys. **3**, 220 (1952). https://doi.org/10.1016/0502-8205(52)90009-9
28. I. Alvarez-Clemares, G. Mata-Osoro, A. Fernandez, et al., Adv. Eng. Mater. **12**, 1154 (2010). https://doi.org/10.1002/adem.201000176
29. Y. Liu, Y. Zhang, K. H. Lim, et al., ACS Nano **12**, 7174 (2018). https://doi.org/10.1021/acsnano.8b03099
30. L. P. Bulat, I. A. Drabkin, V. V. Karataev, et al., Phys. Solid State **52**, 1836—1841 (2010).
31. O. Ivanov, M. Yaprintsev, R. Lyubushkin, and O. Soklakova, Scr. Mater. **146**, 91 (2018). https://doi.org/10.1016/j.scriptamat.2017.11.031
32. M. Yaprintsev, R. Lyubushkin, O. Soklakova, and O. Ivanov, J. Electron. Mater. **47**, 1362 (2018). https://doi.org/10.1007/s11664-017-5940-8
33. F. Wu, H. Z. Song, J. F. Jia, et al., Phys. Status Solidi A **210**, 1183 (2013). https://doi.org/10.1002/pssa.201228589
34. W. Y. Shi, F. Wu, K. L. Wang, et al., J. Electron. Mater. **43**, 3162 (2014). https://doi.org/10.1007/s11664-014-3220-4
35. X. B. Zhao, Y. H. Zhang, and X. H. Ji, Inorg. Chem. Commun. **7**, 386 (2004). https://doi.org/10.1016/j.inoche.2003.12.020

Translated by Sh. Galyaltdinov